Kilo-electron-volt Ar–ion-induced neutral atom desorption from Rh{331}: Relation of angular distributions to surface structure

C. T. Reimann, K. Walzl, and M. El-Maazawi
Department of Chemistry, Pennsylvania State University, University Park, Pennsylvania 16802

D. M. Deaven
Department of Physics, Pennsylvania State University, University Park, Pennsylvania 16802

B. J. Garrison[a] and N. Winograd
Department of Chemistry, Pennsylvania State University, University Park, Pennsylvania 16802

(Received 17 March 1988; accepted 27 April 1988)

The surface structure of single crystal metals in reflected in the angular distributions of neutral atoms desorbed during keV Ar ion bombardment. Results are presented here of a study of desorption from a stepped surface, Rh{331}. Recently, classical dynamics simulations of the desorption process were shown to give excellent agreement with ejection data from Rh{111}, and the same model potential has been used to simulate desorption from Rh{331}. The agreement with experiment remains excellent despite the different coordination of the surface atoms on Rh{111} and Rh{331}. The azimuthal ejection distributions are strongly affected by the steps.

I. INTRODUCTION

Ejection distributions from keV ion-bombarded single crystal metals reflect local structure of the crystal surface.[1] The structural sensitivity arises during the momentum transfer process subsequent to the initial hit by an incident energetic ion.[2] Since surface channeling and blocking of the resultant escaping particles crucially influence the angular details of ejection, the measurement of angle-resolved ejection patterns has been proposed as a new approach for surface studies.[3–5]

The first detailed kinetic energy (KE) and angle-resolved study of desorption from a clean single crystal metal surface bombarded by a low dose of keV ions has recently been reported for Rh atoms ejected from Rh{111}.[6,7] The results of these experiments have proven valuable for comparison to theoretical models of the ion-impact event. The most detailed of these models uses classical dynamical computer simulations. Early calculations utilized pairwise additive interaction potentials to estimate interatomic forces,[7] yielding results in reasonable agreement with experiment, although predicted KE distributions were poorly reproduced. This error presumably arises from complications in describing the interactions in the interfacial region, where the number of neighbor atoms changes rapidly during the desorption event.

A new model potential for classical dynamical simulations of keV ion-induced desorption has recently been developed which is based on the embedded atom method (EAM).[8,9] In the EAM, the potential energy of the ith atom in the lattice is written as $E_i = F[\rho_i = \Sigma_{j\neq i}\rho_{\text{atomic}}(r_{ij})] + 1/2\,\Sigma_{j\neq i}\varphi(r_{ij})$. In this expression, r_{ij} is the distance between the ith and jth atoms, $\varphi(r_{ij})$ is the potential energy of repulsion between the ion cores of the ith and jth atoms, $\rho_{\text{atomic}}(r_{ij})$ is the electron density at the position of the ith atom due to the jth atom, and ρ_i is the total electron density at the position of the ith atom, excluding the electron density provided by the ith atom itself. The embedding function F is a nonlinear function *which is taken not to depend on the source of the electron density.* Thus, once F is determined, it should be usable in an arbitrary configuration of Rh atoms.

The form of the EAM potential may be derived from density functional theory.[10] With this theory, the embedding energy of the ith atom is a functional of the self-consistent electron density with the ith atom removed from the lattice. Two approximations are then made. First, the functional is replaced by a function, and second, the self-consistent electron density is replaced by a homogeneous electron density, the value of which is taken to be the value of the correct density at the position of the ith atom. Finally, a perturbation theory correction is added taking into account the nonuniformity of the electron density near the atom. The result is an expression with the same form as the EAM. (Another correction term, the hybridization or band energy resulting from the formation of delocalized states in the solid,[11,12] is ignored because it would not reflect the actual band structure in the vicinity of a desorption event.) It should be noted that the EAM and the expression from density functional theory are not rigorously identical, so that the EAM is empirical in nature. Also, an alternative interpretation exists for ρ_i.[13] This parameter may be a measure of local density or coordination of atoms[13] rather than a measure of local electron density.[8,9] In either interpretation, however, the atomic interactions are the consequence of many-body forces, which is more realistic for metals than the assumption of pairwise additive potentials.[7]

The empirical manner in which the parameters of a potential and the embedding function F are obtained has been discussed in detail,[14] and a best fit to the Rh{111} ejection data[7] has been obtained.[14] The EAM[14] better accounts for the peak features in the angular and KE distributions than does the pair potential method.[7] Thus, for Rh{111}, the essential features of particle ejection are well accounted for by simple calculations of the collision sequences in the solid.

[a] Camille and Henry Dreyfus Teacher–Scholar.

 0021-9606/88/162539-05$02.10

The simulations confirm simple intuitive notions about how the surface structure determines ejection patterns.

The purpose of this article is to answer the question: Does the EAM account for keV ion-induced desorption from a surface made up of Rh atoms in a configuration unlike that of Rh{111}? The Rh{331} surface is a stepped structure in which a third of the surface atoms are less coordinated than in Rh{111}, and in which another third are more coordinated, as shown in Fig. 1. Perhaps at the step edges, the electronic density is more complicated than is taken into account by a summation of electronic densities contributed by nearby atoms. Moreover, the direction perpendicular to the Rh{331} face, which is the direction in which ions are incident, is a near channeling direction, and it may reasonably be asked what effect this has on the desorption process. To check the effectiveness of the EAM, experimental and theoretical studies were undertaken of ion-induced desorption from the Rh{331} surface. For the simulations, the model potential used was *identical* to that used for Rh{111}.[14] Only the model crystallite was appropriately adjusted.

II. EXPERIMENTAL METHOD

Kinetic energy- and angle-resolved neutral (EARN) desorbed atom measurements are performed using an apparatus previously described.[15] Briefly, desorbed neutral Rh atoms are ionized by multiphoton resonance ionization (MPRI). The pulsed photon source is a tunable Nd:YAG-pumped dye laser with a frequency doubler, operating at a wavelength of 312 nm. Polar angle-resolved detection of the photoionized Rh atoms is achieved in the range $\theta = 0°$ (normal ejection) to $\theta = 90°$ (grazing ejection) using photoion extraction optics and a multichannel plate. A 200 ns pulsed 5 keV Ar^+ ion beam is focused to a 2 mm diameter spot and aimed normally at the Rh{331} sample. After a time delay past each ion pulse, a 6 ns laser pulse, focused into a thin ribbon, is aimed at a known distance from the ion impact point on the target. By varying the time delay between the incident ion pulse and the ionizing laser pulse, a time-of-flight measurement yielding KE-resolved data in the range 0–50 eV is performed on desorbed neutrals. An LSI 11/23 microcomputer software deconvolutes the KE and angular information, providing separately resolved KE and polar angular distributions. The KE resolution is ~4% for 5 eV particles and ~15% for 50 eV particles. The polar angle resolution is ~7%. These resolutions are adequate to measure commonly observed energy and angle distributions. The laser-ionization-based EARN experiment is highly sensitive. In a 15 min run, sufficient to collect a KE- and angle-resolved ejection spectrum, 5×10^{12} ions/cm^2 are incident on the sample, leading to erosion of less than 2.5% of a monolayer. Thus, surface damage by the incident ions is negligible.

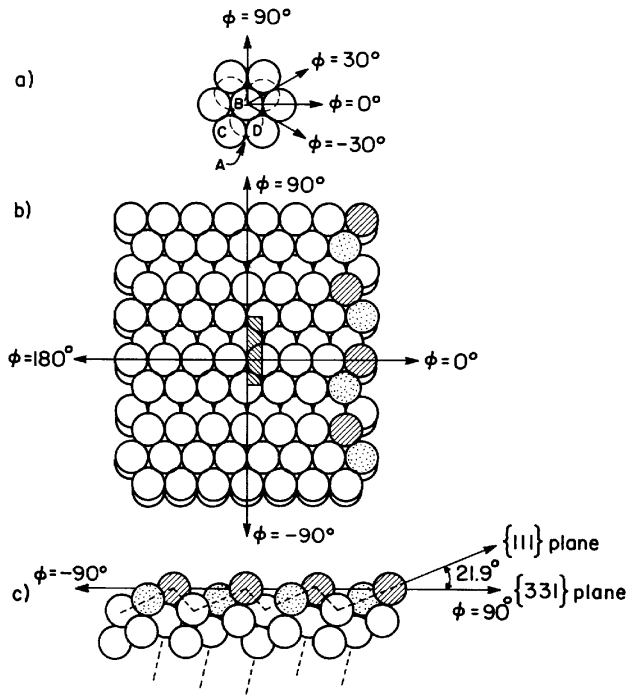

FIG. 1. (a) Rh{111} surface indicating azimuthal directions used in the text. The dashed atoms are in the second layer of the crystal. (b) Rh{331} surface indicating the definition of azimuths used in the text. The $\phi = 0°$ azimuth is the same as that in (a). The impact zone used in the classical dynamical simulation is shown at the center of the crystallite as a shaded box. (c) Rh{331} surface viewed from the $\phi = 0°$ direction. The shaded atoms correspond to the shaded atoms in (b). The dotted near-vertical lines indicate a major channeling direction.

The experiments are performed in a cryopumped ultrahigh vacuum system with a base pressure of $\sim2\times10^{-10}$ Torr. A Rh{331} crystal is mounted on a precision sample manipulator, and azimuthal crystal orientations of $\phi = 90°$, 30°, 0°, − 30°, and − 90° are examined [the coordinate system for these azimuths is shown in Fig. 1(b)]. The sample preparation consists of cycles of 5 keV Ar–ion bombardment using an incident ion beam current of 2 μA, followed by annealing at ~870 °C. Oxygen exposures are used to catalytically remove residual carbon segregated to the surface.[16] This is accomplished by backfilling the chamber with $\sim2\times10^{-7}$ Torr of oxygen and heating the crystal to ~650 °C. After the crystal is flashed to ~1000 °C, the resulting low energy electron diffraction (LEED) pattern is indicative of an ordered Rh{331} surface,[17] and Auger spectroscopy indicates no trace of carbon contaminant. The LEED pattern allows identification of the mirror plane of the surface. The $\phi = +90°$ and $\phi = -90°$ azimuths are distinguished by comparing the measured EARN distributions with the results of classical dynamical simulations.

Simulations were performed on a model Rh{331} crystallite consisting of a total of 540 atoms, arranged in an 8 by 18 atom rectangle. The atoms were bound together by model potential EAM-A, discussed in Ref. 14. The simulations used 3 keV Ar ions instead of the 5 keV ions that were experimentally employed. This was to reduce the size of the model crystalline required to obtain accurate results. The use of lower KE ions in the calculations does not compromise comparison with data, since the collision cascades are larger than the scale of the local structure of the surface. Also, deposited energy is rapidly shared among the target atoms so that by the time desorption occurs, the energy of each target atom is unrelated to the incident ion energy. The desorption yield of edge atoms was 5%–10% of the total, so that the crystallite

contains the collision cascades caused by incident ions. The ions were uniformly incident on an impact zone, shown in Fig. 1(b), which contains all unique impact points on the surface. During each simulation, 1800 ions were incident, resulting in statistically significant ejection features. Simulations were also performed with ions incident perpendicular to the (111) facets of Rh{331} and at a polar angle of $\theta = 21.9°$ along the $\phi = +90°$ azimuth of Rh{111}. In the latter case, the model crystallite of Ref. 14 was used.

III. RESULTS AND DISCUSSION

Polar angle distributions of Rh atoms desorbed from Ar–ion bombarded Rh{331} are presented in Fig. 2(a). These data are integrated in the KE range 10–20 eV. It is seen that ejection is strongly peaked at $\theta = 15°$ along the $\phi = +90°$ azimuth. It is also seen that the $\phi = -30°$ and $\phi = -90°$ azimuths have small but noticeable features at $\theta = 50°$–$60°$. Along the $\phi = 0°$ azimuth of Rh{331}, a small feature is observed at about $\theta = 40°$. The analogous ejection yields from Rh{111}, shown in Fig. 2(b), are characterized by threefold azimuthal symmetry, with dominant ejection along the $\phi = -30°$ and the symmetrically equivalent $\phi = 90°$ azimuth and with off-normal ejection always peaking at about $\theta = 40°$.

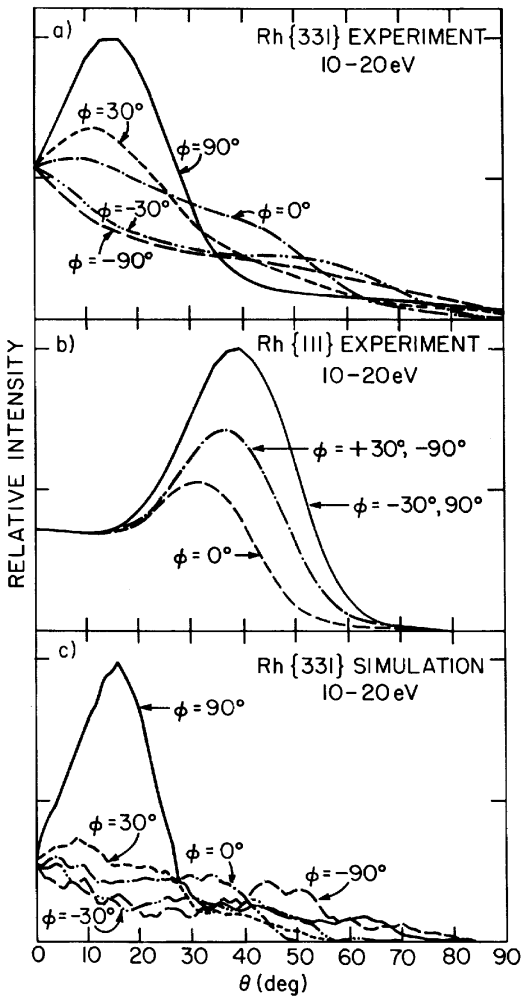

FIG. 2. Polar angle Rh atom distributions of keV ion-induced desorption from Rh single crystals. The 10–20 eV kinetic energy range is shown. (a) Rh{331}, experimental data; (b) Rh{111}, experimental data (Refs. 7 and 14); (c) Rh{331}, calculated curves employing the EAM.

The differences in the ejection patterns between Rh{331} and Rh{111} are related to the different surface structures. There are three notable differences between the structures of Rh{331} and Rh{111}. First, the {111} planes of Rh{331} are tilted 21.9° about the $\phi = 0°$ azimuth with respect to the horizontal {331} surface planes, as shown in Fig. 1(c), whereas in Rh{111} the {111} planes are horizontal. Second, Rh{331} is stepped. Third, the normal direction to Rh{331} is close to a major ion channeling direction, so that Rh{331} is much more "open" than Rh{111}.

The different tilts of the {111} plane for Rh{331} and Rh{111} are of paramount importance in accounting for some of the details of the ejection patterns. The role of the lattice in determining ejection patterns from Rh{111} was previously discussed.[7] The enhanced ejection from Rh{111} along the $\phi = \pm 30°$ azimuths compared to the $\phi = 0°$ azimuth is directly keyed to the registry of the {111} planes. Also, the peaking of polar angle distributions at $\theta = 40°$ for Rh{111} is related to the fact that moving atoms characterized by $\theta \geqslant 40°$ graze the {111} surface and therefore tend to be blocked from ejecting. Finally, some mechanisms of ejection are due to collisional interaction between particular closely spaced second and first layer atoms [A and B of Fig. 1(a)], combined with surface channeling. For these structural effects on particle ejection, the rotation of the lattice between Rh{111} and Rh{331} simply sweeps the ejection feature at $\theta = 40°$ along $\phi = 90°$ to $\theta = 18°$. Thus, the tilt between the lattices of Rh{331} and Rh{111} explains the dominant feature of ejection along the $\phi = 90°$ azimuth from Rh{331} in terms of a similar feature observed for Rh{111}.

Classical dynamics simulations are critical to understanding keV ion-induced desorption. In Fig. 2(c), the results from a simulation of desorption due to 3 keV Ar ions incident on Rh{331} are shown. Several features of the EARN data are successfully accounted for, including (i) the dominant ejection along the $\phi = +90°$ azimuth at $\theta = 15°$ (on the basis of which it is decided what crystal orientation corresponds experimentally to the $\phi = +90°$ azimuth), (ii) the relatively small desorption signal along other azimuths, and (iii) the small desorption features in the range $\theta = 40°$–$60°$ along the $\phi = 0°$, $-30°$, and $-90°$ azimuths. On the other hand, normal ejection is calculated to be lower relative to peak off-normal ejection than is indicated by the data, and the decrease in ejection away from the $\phi = +90°$ azimuth is greater in the simulation than in the data. However, the simulation overall closely resembles the data, and indicates that the EAM potential derived for the Rh{111} crystal results in correct calculations of the dynamics of ejection of surface atoms with considerably different coordination, as in the case of Rh{331}.

Classical dynamical simulations also predict the position of the peak of the KE distributions observed experimentally. Azimuthally averaged KE spectra are observed to peak at 3–5 eV for both Rh{331} and Rh{111}, and the simulation yields a peak at the same KE. Also, the KE spec-

trum of ejection from Rh{331} near $\theta = 15°$ and $\phi = +90°$ maximizes at 7 eV, as does ejection from Rh{111} near $\theta = 40°$ and $\phi = +90°$. Again, the EAM simulation yields a peak at the same KE.

To investigate the roles of lattice orientation, surface steps, and bulk channeling in dictating the details of ejection from Rh{331}, calculations were performed on two other systems: a Rh{331} surface tilted so that ions are incident normal to the {111} facets, and a Rh{111} surface tilted to have the same orientation as the {111} facets of Rh{331} when ions are incident normal to Rh{331}. The tilted Rh{331} surface is analogous to a {111} surface with steps, i.e., with distinct "upstairs" and "downstairs" directions, and the tilted Rh{111} surface is analogous to a Rh{331} crystal with no steps but the same bulk ion channeling as Rh{331}. These geometries are shown in Fig. 3 along with the results of individual trajectories displayed as projections onto a two dimensional surface.

The effect of tilting the {111} faces of the lattices is vividly seen in Fig. 3. For example, the feature α in Fig. 3(d), the "spot" along the $\phi = +30°$ azimuth of Rh{111}, becomes feature β in Fig. 3(a), a slight signal very near the $\phi = 0°$ azimuth. The features experimentally observed in the azimuthal range $\phi = 0°$ to $\phi = -90°$ are a combination of the $\phi = -30°$ and $\phi = -90°$ features from Rh{111}, tilted to higher polar ejection angle θ. Thus, polar and azimuthal ejection features are keyed to the orientation of the lattice, migrating in polar and azimuthal angle in accordance with a 21.9° rotation of the {111} planes about the $\phi = 0°$ azimuth.

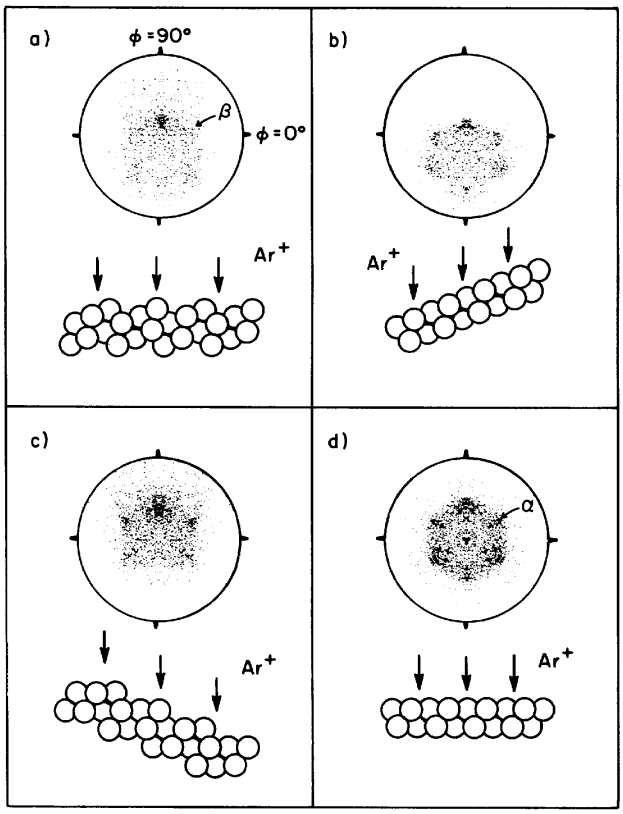

FIG. 3. Spot patterns of desorbed atoms from several stepped, nonstepped, channeling and nonchanneling single crystal surfaces. Each spot represents a desorbed atom and is plotted at a radius of polar angle θ and at an azimuthal angle ϕ. The border corresponds to $\theta = 90°$. This method of plotting spot patterns differs from a previous method (Ref. 18) in which each spot is plotted at a radius of tan (θ) as for a flat plate collector. (a) Ions perpendicularly incident on Rh{331}; (b) ions incident on tilted Rh{111}; (c) ions perpendicularly incident on {111} planes of Rh{331}. The features α and β are discussed in the text.

The results shown in Fig. 3 also elucidate the influence of steps in the desorption process. It is clear that on stepped surfaces, features along the $\phi = 0° - -90°$ azimuths are either attenuated or are spread out over a wider azimuthal range relative to ejection features from flat surfaces. This is independent of the details of the channeling of the incident ions. The steps serve to impede the desorption effect of individual collision cascades which happen to spread along $\phi = -30° - -90°$ azimuths in the {111} planes of Rh{331}. Also, as seen in Fig. 3(c) and 3(d), the ejection along the $\phi = +90°$ azimuth can be enhanced by steps, perhaps because subsurface collision cascades occur closer to the surface downstairs from an ion impact event, with consequently greater ease of ejection.

Channeling significantly reduces the yield of desorbed atoms. For surfaces with the {111} plane tilted 21.9° with respect to the horizontal (such as Rh{331}), the desorption yield (desorbed atoms per incident ion) from the simulation is 1.4 ± 0.2, whereas for surfaces with the {111} plane horizontal (such as Rh{111}), the simulated yield is 3.3 ± 0.2. These trends are qualitatively observed during experiments. Based on the simple Moliere potential,[19] a 3 keV Ar ion has an interaction size of about 0.8 Å, which is small compared to the internuclear Rh atom separation of 2.69 Å. Thus, in the simulations, many ions incident in the near channeling direction penetrate the crystal completely without depositing sufficient momentum to desorb even a single atom.

IV. CONCLUSION

Measurements and classical dynamical simulations of keV ion-induced desorption suggest that desorption from Rh{331} is similar to desorption from Rh{111} if the different tilt of the {111} planes is taken into account. The presence of steps, however, attenuates or broadens ejection features in the azimuthal range $\phi = 0°$ to $-90°$, since desorption must occur through the extra material represented by the steps. Channeling reduces the desorption yield per incident ion by allowing the ions to penetrate deeper into the solid before initiating collision cascades. A many-body interaction potential, previously optimized for the flat Rh{111} surface, also accounts for the Rh{331} data, despite the different coordination of surface atoms between the two cases.

It should be noted that stepped surfaces provide idealized versions of the types of adsorption sites present on the irregular surfaces of supported catalysts. The importance of steps is shown in studies of dissociative adsorption of NO on Rh surfaces. Dissociative NO adsorption occurs readily on Rh{331} but only with difficulty on Rh{111},[20] and probably only at defect sites in the latter case. Also, the order in which various CO binding sites are occupied with increasing CO coverage is different for Rh{331} than for Rh{111}.[21] The "beam" of Rh atoms escaping along the $\phi = +90°$ azimuth could provide a probe for locating adsorbates binding

to threefold hollows of the {111} terraces of Rh{331}, as has been accomplished for the $p(2\times2)$ O/Rh{111} system.[6,22]

ACKNOWLEDGMENTS

The financial support of the Office of Naval Research, the National Science Foundation, and the IBM Program for the Support of the Materials and Processing Sciences is gratefully acknowledged. One of us (B.J.G.) thanks the Camille and Henry Dreyfus Foundation for additional support. The Pennsylvania State University supplied a generous grant of computer time for these studies.

[1]G. K. Wehner, Phys. Rev. **102**, 690 (1956).
[2]D. E. Harrison, Jr., J. P. Johnson III, and N. S. Levy, Appl. Phys. Lett. **8**, 33 (1966).
[3]N. Winograd, B. J. Garrison, and D. E. Harrison, Jr., Phys. Rev. Lett. **41**, 1120 (1978).
[4]N. Winograd, Prog. Solid State Chem. **13**, 285 (1982).
[5]B. J. Garrison and N. Winograd, Science **216**, 805 (1982).
[6]N. Winograd, P. H. Kobrin, G. A. Schick, J. Singh, J. P. Baxter, and B. J. Garrison, Surf. Sci. **176**, L817 (1986).
[7]B. J. Garrison, C. T. Reimann, N. Winograd, and D. E. Harrison, Jr., Phys. Rev. B **36**, 3516 (1987).
[8]M. S. Daw and M. I. Baskes, Phys. Rev. Lett. **50**, 1285 (1983).
[9]M. S. Daw and M. I. Baskes, Phys. Rev. B **29**, 6443 (1984).
[10]M. Manninen, Phys. Rev. B **34**, 8486 (1986).
[11]K. W. Jacobsen, J. K. Nørskov, and M. J. Puska, Phys. Rev. B **35**, 7423 (1987).
[12]J. K. Nørskov, Phys. Rev. B **26**, 2875 (1982).
[13]M. W. Finnis and J. E. Sinclair, Philos. Mag. A **50**, 45 (1984).
[14]B. J. Garrison, N. Winograd, D. M. Deaven, C. T. Reimann, D. Y. Lo, T. A. Tombrello, D. E. Harrison, Jr., and M. H. Shapiro, Phys. Rev. B **37**, 7197 (1988).
[15]P. H. Kobrin, G. A. Schick, J. P. Baxter, and N. Winograd, Rev. Sci. Instrum. **57**, 1354 (1986).
[16]L. A. DeLouise and N. Winograd, Surf. Sci. **138**, 417 (1984).
[17]D. G. Castner and G. A. Somorjai, Surf. Sci. **83**, 60 (1979).
[18]R. A. Gibbs, S. P. Holland, K. E. Foley, B. J. Garrison, and N. Winograd, J. Chem. Phys. **76**, 684 (1982).
[19]G. Moliere, Z. Naturforsch. Teil A **2**, 133 (1947).
[20]L. A. DeLouise and N. Winograd, Surf. Sci. **159**, 199 (1985).
[21]L. A. DeLouise, E. J. White, and N. Winograd, Surf. Sci. **147**, 252 (1984).
[22]C. T. Reimann, M. El-Maazawi, K. Walzl, N. Winograd, and B. J. Garrison (in preparation).